Preprints of the 19th World Congress
The International Federation of Automatic Control
Cape Town, South Africa. August 24-29, 2014

Imaging of Rayleigh damping properties of the *in vivo* brain using parametric Magnetic Resonance Elastography.

Andrii Y. Petrov, Paul D. Docherty, Mathieu Sellier, J. Geoffrey Chase.

Department of Mechanical Engineering, University of Canterbury, Christchurch, New Zealand, (author e-mail: petrov.bme@gmail.com).

Abstract:
The three parameter Rayleigh damping (RD) model applied to time-harmonic Magnetic Resonance Elastography (MRE) has potential to better characterise fluid-saturated tissue systems. However, it is not uniquely identifiable at a single frequency. One solution to this problem involves simultaneous inverse problem solution of multiple input frequencies over a broad range. As data is often limited, an alternative elegant solution is a parametric RD reconstruction, where one of the RD parameters (μ_I or ρ_I) is globally constrained allowing accurate identification of the remaining two RD parameters. This research examines this parametric inversion approach as applied to *in vivo* brain imaging.
Overall, success was achieved in reconstruction of the real shear modulus (μ_R) that showed good correlation with brain anatomical structures. The mean and standard deviation shear stiffness values of the white and gray matter were found to be 3 ± 0.11 kPa and 2.2 ± 0.11 kPa, respectively. Parametric results with globally constrained μ_I indicate that selecting a reasonable value for the μ_I distribution has a major effect on the reconstructed ρ_I image and concomitant damping ratio (ξ_d). More specifically, the reconstructed ρ_I image using a realistic μ_I=333 Pa value representative of a greater portion of the brain tissue showed more accurate differentiation of the ventricles within the intracranial matter compared to μ_I=1000 Pa, and ξ_d reconstruction with μ_I= 330 Pa accurately captured the higher damping levels expected within the vicinity of the ventricles.
Parametric RD reconstruction shows potential for accurate recovery of the stiffness characteristics and overall damping profile of the *in vivo* living brain despite its underlying limitations.

Keywords: Magnetic resonance elastography, inverse problem methods, Rayleigh damping, parametrisation, *in vivo* brain, tissue characterisation, mechanical properties, medical imaging.

1. INTRODUCTION

Because of the diagnostic potential, assessment of the brain tissue mechanical properties has been the subject of several clinical studies (Chatelin et al., 2010). However, the brain is naturally shielded, making it very difficult to accurately investigate viscoelastic (VE) properties, which may prove useful for characterising various brain diseases (Murphy et al., 2011). Additionally, conventional imaging techniques, such as magnetic resonance imaging (MRI), computed tomography (CT) and ultrasonography (US), are not capable of directly assessing mechanical properties of the brain.

Magnetic Resonance Elastography (MRE) can directly visualise and measure tissue elasticity *in vivo* (Lewa and Certaines, 1995). MRE acquisition requires application of mechanical waves to tissue within the MRI and sophisticated inverse problem methods to identify an elastic modulus map of the tissue. Integration of the elastographic imaging with other conventional imaging modalities can bring additional diagnostic potential and enhance understanding of disease mechanisms and progression.

To date, mechanical properties of the brain have been investigated using traditional elastic models, although VE (Kruse et al., 2007; Sack et al., 2007) and poroelastic (PE) (Perriez et al., 2010) models have also been used in different applications. Rayleigh damping (RD) is an alternative model for soft tissue attenuation for elastic materials. Compared to traditional VE models, it incorporates an additional damping parameter proportionally related to the inertial effects (Liu and Gorman, 1995). Thus, the RD model offers a more complex description of energy dissipation using two different forms of damping. Considering the highly-saturated, sponge-like nature of the brain, the RD model may provide a more accurate match to expected brain tissue response.

It has been demonstrated that the RD model is non-identifiable given only single frequency data (Petrov et al., 2013), which is the typical approach in a range of biomedical elastographic inverse problems (Van Houten et al., 2011). However, it should be noted that single frequency data is very appealing venue for MRE as it is fast and only subjects the patient to a single test. This approach has the advantage that repeatability between tests is not

required nor assumed, which could be problematic in multi-frequency tests *in vivo*. Hence, a single frequency approach with reasonable accuracy would offer benefits, if only to obtain good initial estimates. This paper proposes a parametric identification approach to find optimal values in application to *in vivo* elastographic brain imaging with data at a single frequency.

2. MATERIALS & METHODS

2.1 Time-harmonic RD elastography

A linear isotropic nearly-incompressible RD elastic model was applied to *in vivo* sinusoidal brain response to account for the nearly-incompressible behaviour expected in the highly-saturated media like brain tissue. Motion amplitude is calculated from the Navier's equation, which in time-domain is defined:

$$\nabla \cdot (\mu(\nabla \mathbf{u} + \nabla \mathbf{u}^T)) - \nabla(\lambda \nabla \cdot \mathbf{u}) - \nabla P = -\rho \frac{\partial^2 \mathbf{u}}{\partial t^2}, \quad (1)$$

where $\mathbf{u}$ is the displacement within the medium; λ is the first Lamé's parameter, μ is the second Lamé's parameter, also known as a shear stiffness; ρ is the density of the material, ∇P is a pressure term, related to volumetric changes through the bulk modulus, K, via the relationship: $\nabla P = K \nabla \cdot \mathbf{u}$.

The descritised Navier's equation with damping can be represented:

$$\mathbf{M}\ddot{\mathbf{u}} + \mathbf{C}\dot{\mathbf{u}} + \mathbf{K}\mathbf{u} = \mathbf{f}, \quad (2)$$

where $\mathbf{M}$, $\mathbf{C}$ and $\mathbf{K}$ are mass, damping and stiffness matrices, $\mathbf{u}$ is the displacement vector and $\mathbf{f}$ represents known sinusoidal input forcing. In time-harmonic (steady-state) elastography, motion and forces can be defined: $\mathbf{u}(\mathbf{x}, t) = \hat{\mathbf{u}}(\mathbf{x}) e^{i\omega t}$ and $\mathbf{f}(\mathbf{x}, t) = \hat{\mathbf{f}}(\mathbf{x}) e^{i\omega t}$, yielding:

$$(-\omega^2 \mathbf{M} + i\omega \mathbf{C} + \mathbf{K})\hat{\mathbf{u}} = \hat{\mathbf{f}}. \quad (3)$$

In the RD model, the damping is directly proportional to the mass and stiffness, $\mathbf{C} = \alpha \mathbf{M} + \beta \mathbf{K}$, yielding:

$$\left[-\omega^2 \left(1 - \frac{i\alpha}{\omega} \right) \mathbf{M} + (1 + i\omega\beta)\, \mathbf{K} \right] \hat{\mathbf{u}} = \hat{\mathbf{f}}. \quad (4)$$

By assuming stiffness and density to be complex valued, e.g. $\mu^* = \mu_R + i\mu_I$ and $\rho^* = \rho_R + i\rho_I$, Eq. 4 can be further simplified:

$$\Big[-\omega^2 \rho^* \mathbf{M}' + \mu^* \mathbf{K}' \Big] \hat{\mathbf{u}} = \hat{\mathbf{f}}, \quad (5)$$

where $\mathbf{M}' = (1/\rho)\mathbf{M}$ and $\mathbf{K}' = (1/\mu)\mathbf{K}$ are the normalised mass and stiffness matrices, respectively.

μ_R and ρ_R describe the real valued shear modulus and density in the undamped system, while μ_I and ρ_I represent two different damping components related to elastic and inertial effects, respectively; and can be expressed in terms of the RD parameters:

$$\mu_I = \omega \beta \mu_R, \qquad \rho_I = \frac{-\alpha \rho_R}{\omega}. \quad (6)$$

Eq. 6 shows that the μ_I parameter contributes damping linearly proportional to the input frequency and the ρ_I parameter contributes damping inversely proportional to the input frequency. The resulting damping ratio, ξ_d, is defined:

$$\xi_d = \frac{1}{2} \left(\frac{\mu_I}{\mu_R} - \frac{\rho_I}{\rho_R} \right) \quad (7)$$

Rheologically, μ_R and μ_I can be interpreted as the *storage* and *loss* modulus, respectively, while ρ_I for a nearly-incompressible material is hypothesised to indicate fluid perfusion within the solid elastic matrix of the porous media causing energy loss due to the mass transfer.

Thus, the RD model allows reconstruction of not only the stiffness distribution (μ_R), but also energy attenuation mechanisms proportionally related to both elastic (μ_I) and inertial (ρ_I) effects. Accounting for two damping mechanisms may allow better description of the microscale interactions that cause motion attenuation in brain tissue, compared to the more commonly used VE models, which do not incorporate inertial damping effects.

2.2 Parametric-based identification

Full simultaneous three-parameter RD reconstruction is not identifiable with single frequency input data (Petrov et al., 2013). Collecting $\Re$ and $\Im$ terms from Eq. 5, yields:

$$\Big[(\mu_R - \omega^2 \rho_R) + i(\mu_I - \omega^2 \rho_I) \Big] \hat{\mathbf{u}} = \hat{\mathbf{f}}. \quad (8)$$

Assuming a known ρ_R value, Eq. 8 implies that μ_R is uniquely identifiable as a direct function of the real displacements: $\mu_R = \hat{\mathbf{f}}_R / \mathbf{u}_R + \omega^2 \rho_R$. However, the model behaviour dictated by the imaginary part of the $\hat{\mathbf{u}}$ coefficient is determined by two model parameters, ρ_I and μ_I, which are both variables to be identified. Hence, both parameters have a model role, but there cannot be unique identification of those variables at one frequency without further *a-priori* information.

In a parametric RD inverse problem approach either ρ_I or μ_I is set to a constant value or dependant function. This approach eliminates a variable, yielding a uniquely identifiable system of one equation with one unknown for $\mathbf{u}_I$ in Eq. 8. However, it restricts the solutions generality.

2.3 Subspace-based nonlinear inversion (SNLI)

The 3D subspace-based nonlinear inversion (SNLI) algorithm (Van Houten et al., 2001) calculates the final property estimates through an iterative optimization framework that minimises the objective function (Φ) defined:

$$\Phi(\boldsymbol{\theta}) = \sum_{i=1}^{N_m} (\mathbf{u}_i^m - \mathbf{u}_i^c(\boldsymbol{\theta}))(\mathbf{u}_i^m - \mathbf{u}_i^c(\boldsymbol{\theta}))^H, \quad (9)$$

where $\mathbf{u}_i^m$ represents the complex valued measured displacement data at i'th measurement point, $\mathbf{u}_i^c(\boldsymbol{\theta})$ is the co-located displacement calculated by a forward simulation of the model using a current estimate of the properties ($\boldsymbol{\theta}$), N_m is the number of measurements and the superscript ^{H} denotes the complex conjugate transpose. The conjugate-gradient (CG) method is used to iteratively update the material property distribution by improving the agreement between finite element (FE) computed displacements and the displacements captured by MRI.

2.4 In vivo brain MRE experimental data

Parametric RD reconstructions were performed on a healthy volunteer of a 24 years old. Ethics approval was obtained from the Institutional Review Ethics Board of the University of Illinois at Urbana-Champaign (Urbana, Illinois, USA). Informed consent was obtained prior the MRE examination.

MRE experiments were performed using a 3T Allegra head-only scanner (Siemens Medical Solutions, Erlangen, Germany). 3D motion encoding was achieved by an innovative multi-shot spin-echo (SE) sequence with bi-polar spiral motion encoding gradients (MEGs) (Johnson et al., 2013). 20 coronal slices of $2 \times 2 \times 2$ mm isotropic voxel resolution were acquired using following parameters: 6 k-space interleaves, time to repetition (TR) / time to echo (TE) = 2000/55 ms, field of view (FOV) = 256 mm, 128×128 matrix resolution. Wave acquisition was performed by 8 equally spaced time harmonics over a single period. Complex-valued subtraction was used to combine images with positive and negative gradient polarisation. Fast Fourier Transform (FFT) was applied to extract motion at a first harmonic which resulted in 3D complex-valued displacements. No further filtering was applied to the data prior to reconstruction processing. Total MRE acquisition time was less than 10 minutes. The quality of each MRE data set was evaluated by calculating octahedral shear strain SNR (OSS-SNR) (McGarry et al., 2011).

The actuation system comprised a long rod that was mutually attached to a speaker membrane at one end and a custom-made cradle on which the head was positioned on the other end. A 50 Hz excitation frequency was applied resulting strong deflection component of the head motion parallel to the head-feet direction.

2.5 Reconstruction protocol

The SNLI algorithm was used to estimate material properties from measured MR displacement data. Reconstruction computations were carried out on High Performance Computing (HPC) system *Blue Fern P575*. A total of 32 processors were employed in a parallel Message Passing Interface (MPI) environment using CG optimisation method. The average runtime for the reconstruction processing was 5 hours. Each parameter was interpolated at different resolution levels.

Reconstruction of material properties using an isotropic linearly elastic nearly-incompressible RD model was performed using the following parameters: an isotropic subzone size of $24 \times 24 \times 24$ mm with the subzone overlap of $0.15 \times 0.15 \times 0.15$ %. Initial and final total variation minimisation (TVM) weighting was 10^{-15} and 10^{-14} with TVM delta set to 10^{-19}. The initial and final spatial filtering (SF) weights were set to 0.25 % and 0.15 % respectively. Displacements were approximated on the mesh with $1.8 \times 1.8 \times 1.9$ mm voxel resolution, providing approximately 16 nodes per wavelength for the FE forward problem. Initial *a-priori* estimates were: μ_R = 3300 Pa and ρ_I = -100 kg/m^3. To allow parametric RD reconstruction, μ_I was globally constrained and excluded from the identification with the values of 330 Pa and 1000 Pa. To account for a nearly-incompressible behaviour expected in a highly saturated media like brain tissue, the density (ρ_R) and the bulk modulus (K) were constrained from inversion and set to 1000 kg/m^3 and 10^7 Pa, respectively.

Convergence criteria was achieved for all material properties for brain reconstruction. Stabilisation of statistical indicators (median and interquartile range (IQR)) of parameter behaviour across all the nodes within the finite element mesh (FEM) was used to evaluate of the convergence for a particular parameter.

3. RESULTS

Figure 1 shows parametric-based RD reconstruction results of the *in vivo* healthy brain with globally constrained μ_I=333 Pa and with μ_I=1000 Pa. Figures 1 (a) and 1 (b) shows a T1-weighted MP-RAGE MR image of the brain within *corpus callosum* for anatomical reference. The structure of the ventricles, depicted by relatively low μ_R values compared to the white / gray matter regions, can be distinguished in the μ_R image (refer to Figures 1 (c) and 1 (d)).

Reconstruction results indicate that selecting reasonable value for μ_I distribution has a major effect on the reconstructed ρ_I image and concomitant ξ_d image. More specifically, the reconstructed ρ_I image with a more realistic μ_I=333 Pa value representative of a greater portion of the brain tissue showed more accurate differentiation of the fluid-filled ventricles within the intracranial matter (refer to Figure 1 (f)) compared to the estimated ρ_I image with μ_I=1000 Pa (refer to Figure 1 (e)). The location and geometry of the ventricles on the ρ_I image with μ_I=333 Pa partially correlates with the location and geometry of the ventricles on the MR image only in the lower slices. However, the upper slices of the brain where the structure of the ventricles is no longer present still captured areas with increased ρ_I values indicating inaccurate reconstruction results.

Consequently, the calculated ξ_d image with μ_I= 333 Pa (refer to Figure 1 (h)) captured relatively higher expected damping levels within the vicinity of the ventricles more accurately compared with the ξ_d image with μ_I=1000 Pa (refer to Figure 1 (g)). The latter indicated scattered distributions of the higher damping levels throughout the intracranial tissue indicating inaccurate locally resolved damping properties. In both images, regions of increased ξ_d values generally correlate with the regions of increased ρ_I values.

4. DISCUSSION

4.1 RD reconstruction results

This investigation assessed the efficacy of the parametric RD model to accurately estimate elastic and damping characteristics of an *in vivo* healthy brain by noting the ability of the algorithm to capture the complex geometry of the brain structure. The results present qualitative evidence that parametric RD model applied to MRE is able to resolve local variations in tissue stiffness, as well as damping profile that correlate with brain anatomical structures. The results also indicate limited applicability

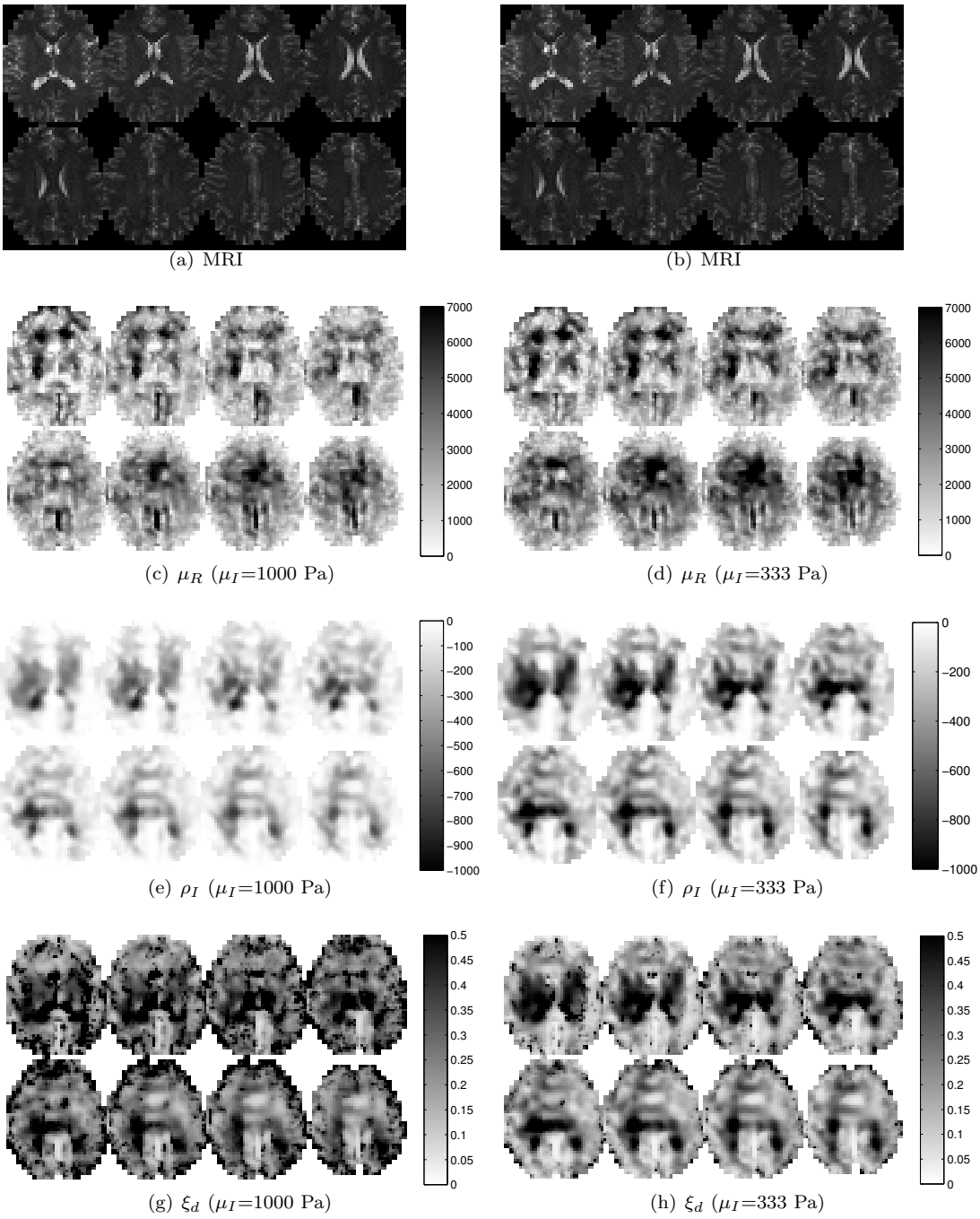

(a) MRI (b) MRI

(c) μ_R (μ_I=1000 Pa) (d) μ_R (μ_I=333 Pa)

(e) ρ_I (μ_I=1000 Pa) (f) ρ_I (μ_I=333 Pa)

(g) ξ_d (μ_I=1000 Pa) (h) ξ_d (μ_I=333 Pa)

Fig. 1. Image results for parametric-based RD reconstruction of the same *in vivo* healthy brain at 50 Hz with globally defined μ_I=1000 Pa (left column) and μ_I=333 Pa (right column): (a) and (b) T1-weighted MP-RAGE MRI image of the brain; (c) and (d) storage modulus μ_R image (Pa); (e) and (f) imaginary density ρ_I image (kg/m^3); and (g) and (h) damping ratio ξ_d image (%).

Table 1. Current mechanical property estimates of brain tissue by MRE using nonlinear inversion (NLI) algorithm, direct inversion (DI) approach and local frequency estimation (LFE) algorithm.

Brain MRE (kPa)	Inversion	ω (Hz)	μ_R (kPa)	μ_I (kPa)
RD model	NLI			
White matter		50	3	0.46
Gray matter		50	2.1	0.3
Curtis *et al* (2012)	NLI			
White matter		50	2.66	0.3
Gray matter		50	2.02	1.04
Wuerfel *et al* (2009)	DI			
White / Gray Matter		50	1.6	0.65
Green *et al* (2008)	DI			
White matter		60	2.7	2.5
Gray matter		60	3.1	2.5
Kruse *et al* (2008)	LFE			
White matter		100	13.6	NA
Gray matter		100	5.22	NA
Sack *et al* (2009)	PWI			
White / Gray matter		50	1.5	0.6
White / Gray matter		62.5	2	0.8
Sack *et al* (2008)	PWI			
White / Gray matter		25	1.17	3.1 Pa
White / Gray matter		50	1.5	3.4 Pa
Vappou *et al* (2007)	PWI			
White / Gray matter		80	1.15	0.91
White / Gray matter		100	1.13	0.93
White / Gray matter		120	1.19	1.01
White / Gray matter		140	1.22	1.07
McCracken *et al* (2006)				
White matter		TP	12	NA
Gray matter		TP	8	NA
Uffman *et al* (2004)	DI			
White matter		80	15.2	NA
Gray matter		80	12.9	NA

of the parametric RD model to accurately characterise viscoelastic properties of the brain tissue due to the obvious limitations associated with parametric approach. Hence, further studies using brain phantoms and multifrequency RD elastography are required.

In the parametric RD model formulation, only μ_R can be accurately recovered from the displacement data of single frequency, as it is uniquely identifiable provided the density of the brain tissue is the same of a water. Qualitatively, the estimated μ_R distribution showed good correlation with the white & gray matter and ventricles located in the centre of the brain. The outer brain regions in the vicinity of gray matter appear to be stiffer compared to the inner brain parenchyma in vicinity of white matter, which correlates well with the previously reported results (Sack et al., 2007; Klatt et al., 2007; Vappou et al., 2007). The mean and standard deviation (STD) μ_R values for white and gray matter were found to be 3 ± 0.11 kPa and 2.2 ± 0.11 kPa, respectively. Table 1 provides comparison between previously reported mechanical properties of the *in vivo* brain estimated by MRE and current estimates computed by SNLI based RD material model.

Lower shear modulus values within the ventricles confirm rapid attenuation of the shear strain waves within the CSF. The latter could be described as Newtonian viscous fluid, with viscosity 0.7 - 1 mPa.s, which leads to a nearly zero elasticity in μ_R values, as well as viscosity in μ_I values. Although fluid-filled ventricles have not been reconstructed with nearly zero μ_R values, they are still much lower than the surrounding brain tissue, which is plausible. Generally, μ_R decreases in the area of the ventricles, while the magnitude of the ξ_d increases. The results justify the expected identifiably of the μ_R parameter within the model formulation and its independence from the imaginary components, μ_I and ρ_I.

The connection between the values for ρ_I and anatomical structure is less obvious. However, some correlation is still evident. It is important to recapitulate that rheologically ρ_I maps show regions where the form of fluid damping is dominant compared to elastic shear wave attenuation. This hypothesised behaviour is confirmed by the relatively high ρ_I values in the vicinity of the ventricle structures, and implies increased attenuation due to the fluidic damping in these regions. No significant variations in ρ_I image correlating with differentiation between white and gray matter was noted. Further studies may elucidate a connection between ρ_I and various decease state. However, this preliminary study is only concerned with achieving accurate reconstruction of RD parameters.

4.2 OSS-SNR

Quantification of the noise provides information about the quality of measured motion data, where high SNR improves reconstruction accuracy. Achieving high SNR in the living *in vivo* brain is challenging due to the natural shielding effects of the skull, meninges and CSF in which the brain is submerged (Sack et al., 2007). Previous studies of the OSS-SNR showed accurate shear stiffness reconstructions of the tissue-simulating phantom materials at strain SNR above threshold of 5. In feline brain studies, the reconstructed shear stiffness values were stabilised at a strain SNR above 3 (McGarry et al., 2011). These results suggested a reliable threshold of 3 for the strain SNR to achieve accurate elastographic reconstructions.

In this research, the particular actuation methodology as well as correction for rigid body motion (RBM) induced phase-errors resulted in high quality motion data with average OSS-SNR value of ~ 4.5, which is above previously established threshold value of ~ 3.0 for accurate inversion. High OSS-SNR value was observed even in the middle of the brain where motion undergoes significant attenuation. Therefore, the noise in the displacements fields is not expected to influence accuracy of the elastographic results.

4.3 Limitations

Damping in biological tissues occurs due to the complex, multiscale interactions, such as friction, scattering, and dispersion between microstructural tissue elements. Any biomechanical model approximates a material as a continuum and therefore has limitations in its ability to comprehensively assess underlying attenuation mechanisms. Since the RD model is able to differentiate between two classes of attenuation originating from different structural effects, it may be able to provide a more generalised description of the elastic energy dissipation within the brain. It could thus improve the accuracy and performance of elastographic reconstruction.

Although able to account for an additional damping component arising from inertial effects, compared to traditional VE models, the RD model is still expected to produce artefacts in elastic property reconstruction of real biological tissue. This loss of accuracy occurs because, in general, overall damping forces include additional components, among elastic and inertial ones, that are not included in the RD model.

It is also important to emphasise that the ability of the model to reproduce observed mechanical response can only be as good the fundamental assumptions that underly model formulation. In this research, the brain tissue is assumed to be a linear isotropic nearly-incompressible RD elastic continuum. However, the real *in vivo* brain is known to be a highly heterogeneous, orthotropic, fluid-saturated medium (Prange et al., 2000). Therefore, the reconstruction results may also be inaccurate due to fundamental data-model discrepancy.

In parametric RD reconstruction of heterogeneous tissues, such as the brain, constraining μ_I to a single global value throughout the reconstruction domain presents obvious limitation with regards to accurate *a-priori* information for various tissue types characterised by different mechanical properties. A more advanced parametric inversion approach would include specification of multiple regions of interest (ROIs) associated with a particular tissue type where specific *a-priori* values for the material properties can be defined for each individual region. Segmentation of different tissues will allow more accurate local definition of the material properties and thus improve parametric based RD elastographic reconstruction.

5. CONCLUSIONS

This research presents parametric-based results for RD model based brain MRE. Overall, RD MRE using a parametric approach showed some benefit for qualitative characterisation of the material property distributions, as well as measurable limitations related to accurate identification of the imaginary RD parameters at a single frequency. Full identifiability of the model may be possible via multiple excitation frequencies over a broad range. Parametrisation examining results across a broad range of assumed values, with or without ROIs can be also performed. The success achieved here in elastic property reconstruction indicates that the method is a potentially valuable approach to medical imaging.

6. ACKNOWLEDGMENTS

The authors would like to acknowledge Dr. Curtis L. Johnson from the Department of Mechanical Science and Engineering, University of Illinois at Urbana-Champaign, (Urbana, Illinois, USA) for help in data collection.

7. CONFLICT OF INTEREST STATEMENT

We declare that we have no conflicts of interest.

REFERENCES

Chatelin, S., Constantinesco, A., and Willinger, R. (2010). Fifty years of brain tissue mechanical testing: from in vitro to in vivo investigations. *Biorheology*, 47(5), 255–276.

Johnson, C., McGarry, M., Van Houten, E., Weaver, J., Paulsen, K., Sutton, B., and Georgiadis, J. (2013). Magnetic resonance elastography of the brain using multishot spiral readouts with self-navigated motion correction. *Magnetic Resonance in Medicine*, 70(2), 404–412.

Klatt, D., Hamhaber, U., Asbach, P., Braun, J., and Sack, I. (2007). Noninvasive assessment of the rheological behavior of human organs using multifrequency mr elastography: a study of brain and liver viscoelasticity. *Physics in Medicine and Biology*, 52(24), 7281–7294.

Kruse, S.A., Rose, G.H., Glaser, K.J., Manduca, A., Felmlee, J.P., Jack, C.R., and Ehman, R.L. (2007). Magnetic resonance elastography of the brain. *Neuroimage*, 39(1), 231–237.

Lewa, C.J. and Certaines, J.D. (1995). Mr imaging of viscoelastic properties. *Journal of Magnetic Resonance Imaging*, 5(2), 242–244.

Liu, M. and Gorman, D. (1995). Formulation of rayleigh damping and its extensions. *Computers & structures*, 57(2), 277–285.

McGarry, M., Van Houten, E., Perrinez, P., Pattison, A., Weaver, J., and Paulsen, K. (2011). An octahedral shear strain-based measure of snr for 3d mr elastography. *Physics in Medicine and Biology*, 56, N153.

Murphy, M.C., Huston, J., Jack, C.R., Glaser, K.J., Manduca, A., Felmlee, J.P., and Ehman, R.L. (2011). Decreased brain stiffness in alzheimer's disease determined by magnetic resonance elastography. *Journal of Magnetic Resonance Imaging*, 34(3), 494–498.

Perriez, P., Kennedy, F., Van Houten, E., Weaver, J., and Paulsen, K. (2010). Magnetic resonance poroelastography: an algorithm for estimating the mechanical properties of fluid-saturated soft tissues. *Medical Imaging, IEEE Transactions on*, 29(3), 746–755.

Petrov, A.Y., Geoffrey Chase, J., Sellier, M., and Docherty, P.D. (2013). Non-identifiability of the rayleigh damping material model in magnetic resonance elastography. *Mathematical biosciences*, 246(1), 191–201.

Prange, M., Meaney, D., Margulies, S., et al. (2000). Defining brain mechanical properties: effects of region, direction, and species. *Stapp car crash journal*, 44, 205.

Sack, I., Beierbach, B., Hamhaber, U., Klatt, D., and Braun, J. (2007). Non-invasive measurement of brain viscoelasticity using magnetic resonance elastography. *NMR in Biomedicine*, 21(3), 265–271.

Van Houten, E.E.W., Miga, M.I., Weaver, J.B., Kennedy, F.E., and Paulsen, K.D. (2001). Three-dimensional subzone-based reconstruction algorithm for mr elastography. *Magnetic Resonance in Medicine*, 45(5), 827–837.

Van Houten, E., McGarry, M., Perrinez, P., Perreard, I., Weaver, J., and Paulsen, K. (2011). Subzone based magnetic resonance elastography using a rayleigh damped material model. *Medical Physics*, 38, 1993.

Vappou, J., Breton, E., Choquet, P., Goetz, C., Willinger, R., and Constantinesco, A. (2007). Magnetic resonance elastogrpahy compared with rotational rheometry for in vitro brain tissue viscoelasticity measurements. *Magnetic Resonance Materials in Physics, Biology and Medicine*, 20, 273–278.